COMMUNICATION

X-ray absorption resonances near L$_{2,3}$-edges from real-time propagation of the Dirac–Kohn–Sham density matrix

Marius Kadek,[a] Lukas Konecny,[b] Bin Gao,[a] Michal Repisky*[a] and Kenneth Ruud*[a]

The solution of the Liouville–von Neumann equation in the relativistic Dirac–Kohn–Sham density matrix formalism is presented and used to calculate X-ray absorption cross sections. Both dynamical relaxation effects and spin–orbit corrections are included, as demonstrated by calculations of the X-ray absorption of SF$_6$ near the sulfur L$_{2,3}$-edges. We also propose an analysis facilitating the interpretation of spectral transitions from real-time simulations, and a selective perturbation that eliminates nonphysical excitations that are artifacts of the finite basis representation.

X-ray absorption spectroscopy (XAS) is a powerful technique to determine the structural and electronic properties of matter at the atomic level, in which core electrons are excited to unoccupied or continuum states after absorbing photons in the X-ray energy range. The resulting absorption peaks, normally called edges in XAS, are conventionally labeled according to the originating core state, for instance K-edge for 1s, L$_1$-edge for 2s, L$_2$-edge for 2p$_{1/2}$ and L$_3$-edge for 2p$_{3/2}$, and the spectrum near these edges is called X-ray absorption near-edge structure (XANES). The involvement of core electrons brings great challenges for theoretical studies of XAS because core–valence excitations have to be described. Methods for calculating XAS spectra have been developed for many decades, and several approaches have been proposed: the static exchange approximation,[1] the multiple scattering methods,[2,3] the Bethe–Salpeter equation,[4–6] and different *ab initio* methods (such as the coupled cluster[7] and second-order algebraic-diagrammatic construction model[8]), to name just a few. Time-dependent density functional theory[9] (TDDFT) has proved to be economic for calculating electronic excitations,[10] but its application to XAS is prohibitively expensive except for small molecules, as a large number of roots must be determined in order to access the high-energy excitations. Several solutions have been proposed to

circumvent this difficulty, such as the restricted excitation window TDDFT (REW-TDDFT)[11,12] or the complex polarization propagator approach.[13–15]

In this work we examine an alternative route to the simulation of X-ray absorption processes near the L$_{2,3}$-edges. The essence of the approach is the combination of a rigorous relativistic formalism based on the Dirac–Coulomb Hamiltonian with the real-time formulation of TDDFT (RT-TDDFT). In contrast to previous methods based on linear-response TDDFT (LR-TDDFT), the present real-time approach also offers the possibility to simulate a wide range of spectroscopic techniques involving strong electromagnetic fields while at the same time variationally accounting for all indispensable relativistic corrections, of which the spin–orbit (SO) coupling is of significant importance, as manifested by the multiplet structure of the spectral lines near/at L$_{2,3}$ absorption edges. Although the RT-TDDFT formalism has already been used for modeling core-level absorption spectroscopy of molecular systems,[16–20] in this work we present the first application of the approach at the relativistic 4-component level of theory with the variational inclusion of SO corrections. The usefulness of such a method has been examined on hydrogen-like systems by Selstø *et al.*[21] and in the perspective on relativistic quantum chemistry by Belpassi *et al.*[22]

Furthermore, in this Letter we address two shortcomings of current applications of RT-TDDFT to XAS. One problem is that the comparison of high-energy excitations with experiment can often be hampered by competing excitation processes, some of which are artifacts of treating the excitations in a finite basis set that cannot properly describe excitations to the continuum. By restricting the perturbation operator, we significantly reduce the intensity of such artificial transitions, thus identifying the genuine core excitations. The second difficulty is to classify and interpret the characters of the transitions, for which there is no unique and straightforward way in real-time simulations. To overcome this issue, we introduce the dipole-weighted transition analysis (DWTA). Finally, we assess the methodology on the XAS of the SF$_6$ molecule near the sulfur L$_{2,3}$-edges, and compare the theoretical spectrum with available high-resolution experimental data.[23]

[a] Centre for Theoretical and Computational Chemistry, Department of Chemistry, University of Tromsø—The Arctic University of Norway, N-9037 Tromsø, Norway. E-mail: kenneth.ruud@uit.no, michal.repisky@uit.no; Tel: +47 77623101

[b] Department of Inorganic Chemistry, Faculty of Natural Sciences, Comenius University, Bratislava, Slovak Republic

The central equation of motion of (RT-)TDDFT in the formalism of the density matrix is the Liouville–von Neumann equation, which reads (in atomic units)

$$i\frac{\partial D(t)}{\partial t} = [F(t), D(t)], \tag{1}$$

where the one-electron reduced density, $D(t)$, as well as the mean-field Dirac–Fock operator, $F(t) = F[t, D(t)]$, are assumed to be represented in the orthonormal basis of ground-state molecular spin–orbitals (MOs).

A numerically stable and robust solver of eqn (1) should preserve essential properties of the density matrix, such as trace (number of electrons) and idempotency.[24,25] Our implementation consists of two main components: (1) the second-order mid-point Magnus solver, which is based on the truncation and approximation of the Magnus expansion of the evolution operator.[26] (2) An extrapolation–interpolation scheme,[27] required by the nonlinear [in terms of $D(t)$] character of eqn (1). The latter proved important for ensuring the stability of the time propagation.

To compute the X-ray absorption spectrum from an RT-TDDFT simulation, we first perform a time-independent DFT calculation to obtain the reference ground-state density matrix D_0. The initial perturbed density matrix $D(0^+)$ is obtained from the ground-state density matrix using

$$D(0^+) = \exp(i\kappa P_{\mathbf{n}})D_0 \exp(-i\kappa P_{\mathbf{n}}), \tag{2}$$

which corresponds to an analytic form of an applied Dirac delta-function type external potential in the dipole approximation; i.e. $F(t) = F_0(t) - \kappa\delta(t)P_{\mathbf{n}}$, where $F_0(t)$ is the unperturbed Dirac–Fock operator, κ the magnitude of the field, and $P_{\mathbf{n}}$ the electric dipole moment operator projected onto the direction of the field $\mathbf{n}$. Eqn (2) can be proved using the integral form of eqn (1), see ref. 27.

During the time propagation of the perturbed state, we calculate the induced dipole moment on-the-fly, which is then Fourier transformed and used to calculate the field-dependent dynamical dipole polarizability tensor $\alpha(\omega)$. The final absorption spectrum of a compound is the dipole strength function $S(\omega)$ obtained from the polarizability tensor as

$$S(\omega) = \frac{4\pi\omega}{3c}\text{ImTr}[\alpha(\omega)], \tag{3}$$

where c is the speed of light.

We have implemented the relativistic four-component RT-TDDFT method in the ReSpect program,[28] and the implementation combines the Dirac–Coulomb Hamiltonian with the non-relativistic adiabatic DFT exchange–correlation functionals, of which the hybrid B3LYP functional was applied in the present work.[29,30] The DFT contributions were evaluated numerically on an adaptive molecular grid and their rotational invariance was preserved by means of a non-collinear approach with the spin density described by the norm of the spin magnetization vector. The molecular geometry was optimized at the four-component level of theory ($r_{\text{S–F}} = 1.60753$ Å; experimental value[31] is 1.564 Å) using the ReSpect program package,

employing for the large component uncontracted all-electron Gaussian-type basis sets of triple-zeta quality (cc-pVTZ).[32] The small-component basis was generated on-the-fly imposing the restricted kinetically balanced relation.[33] In the RT-TDDFT simulations, we used the calculated molecular geometry along with an augmented version of the correlation-consistent basis family; aug-cc-pV(T+d)Z for sulfur[34] and a modified aug-cc-pVTZ for fluorine (all f and the most diffuse d functions were removed).[35] For all nuclei, a finite-sized Gaussian model was used. The X-ray absorption spectrum of SF_6 was obtained from RT-TDDFT such that the electronic ground state was perturbed using an analytic δ-function pulse with strength $\kappa = 0.0005$ au and evolved for 56 000 time steps of length 0.025 au (≈ 0.6 attoseconds), this corresponds to a total simulation time of approximately 34 fs and leads to an energy (frequency) resolution of 122 meV in the calculated spectrum. An average wall-clock time per time step was 36.1 seconds, where each step requires two Fock matrix constructions and two matrix diagonalizations—the implementation details can be found in ref. 27. To account for the error caused by the finite-simulation length, we artificially damped the time signal with an exponential function $\exp(-\gamma t)$, $\gamma = 0.0038$ au before its Fourier transformation, resulting in broadened Lorentzian-shaped peaks. This damping is not related to genuine lifetimes of excited states which remain infinite in the present theoretical model. The spectrum is normalized in accordance with experiment[23]—the intensity of the first peak equals one. The final figures were plotted using Python's matplotlib library.[36]

TDDFT calculations in a finite basis representation introduce the two following problems in order to correctly predict the XANES experiment: first, DFT exchange–correlation (XC) functionals tend to underestimate excitation energies due to the self-interaction error and the associated integer discontinuity in the derivative of the total energy with respect to the number of electrons.[37] However, this problem manifests itself only in a global, frequency-independent offset of the excitation energies, which is then corrected by uniformly shifting the entire spectrum by a constant. In our case, we shifted the calculated spectrum by 7.89 eV to match the first experimental peak. We note, that this correction accounts for various deficiencies of the density functional theory, such as the incomplete description of dynamical relaxation or self-interaction errors. The second problem is the emergence of non-physical transitions from non-core occupied orbitals to high-laying virtual orbitals. These peaks often appear in the XANES region as artificial peaks and prevent the interpretation of simulated spectra. We observe on SF_6 that restricting the perturbation electric dipole moment operator $P_{\mathbf{n}}$ only to excitations from sulfur 2p core spin–orbitals suppresses the intensities of the artificial peaks by several orders of magnitude. Furthermore, intensities of resonances in the energy region below 170 eV were also reduced, while leaving the genuine L-edge transitions unaltered. We will refer to the restriction of the perturbation operator as selective perturbation (SP), which is easily implemented by keeping nonzero only those $P_{\mathbf{n},ai}$ matrix elements for which i denotes occupied core orbitals, and a spans all virtuals, thus formally
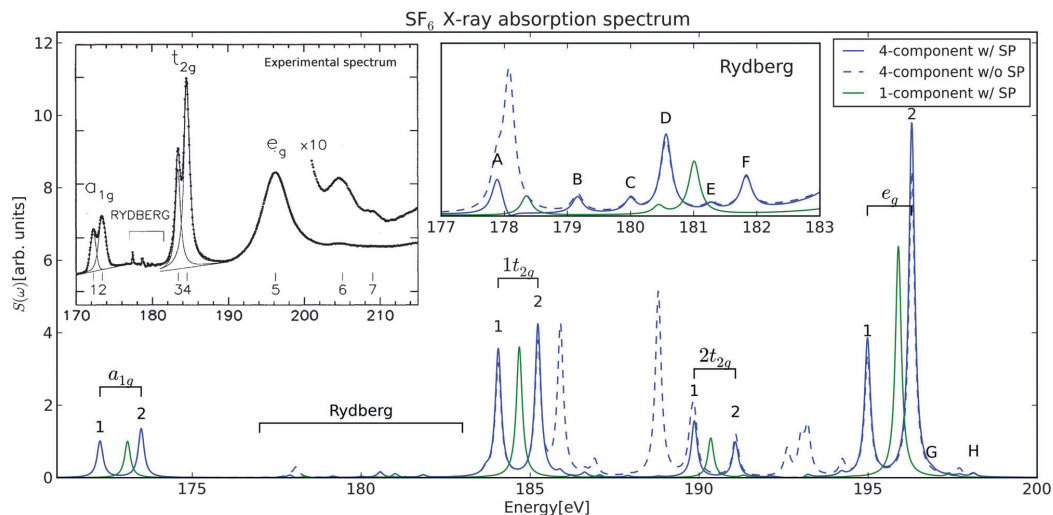
Fig. 1 The photoabsorption spectrum of SF_6 near the sulfur $L_{2,3}$-edges. Fourier-transformed data was fitted using Lorentzian functions to obtain the spectrum; the normalization is the same as in experiment. Continuous lines: results of the calculations with the selective perturbation (SP) restricted only to core sulfur $2p_{1/2}$ and $2p_{3/2}$ spin–orbitals. Dashed line: results of the calculation with the full perturbation. Peaks without a label represent excitations from non-core occupied orbitals to high-lying virtual spin–orbitals.

making transitions between any other orbitals dipole forbidden. It is important to note that we do not reduce the dimensions of the matrices, preserving the orbital relaxation orbitals, as opposed to the alternative approach taken in REW-TDDFT. Moreover, the selective perturbation is not limited to real-time methods, and can also be applied in the LR-TDDFT approach. The contrast in calculated XANES spectra of SF_6 with SP (continuous line) and without SP (dashed line) is depicted in Fig. 1.

An additional known weakness of real-time simulations is any interpretation of resonances. In order to determine the nature of a particular electronic excitation in terms of transitions between molecular orbitals, and also to prove that the peaks suppressed due to the SP correspond to non-core excitations, we propose the dipole-weighted transition analysis (DWTA). This approach is based on a Fourier transform of the partial contributions of an occupied-virtual spin–orbital pair ia to the dynamic polarizability:

$$\alpha_{\mathbf{n},\mathrm{ai}}(t) = \frac{1}{\kappa}\left[P_{\mathbf{n},\mathrm{ia}}D_{\mathrm{ai}}(t) + P_{\mathbf{n},\mathrm{ai}}D_{\mathrm{ia}}(t)\right]. \tag{4}$$

We note that a Fourier component of the density matrix $D_{\mathrm{ai}}(\omega)$ in the real-time formalism is essentially the response matrix obtained from the solution of the LR-TDDFT equation, provided that a small external field was used (linear response regime). A resonant Fourier component $D_{\mathrm{ai}}(\omega_{\mathrm{exc}})$ contains information about transitions between molecular spin orbitals, allowing the analysis of a spectral line with excitation energy ω_{exc} in terms of these transitions. Finally, we visualize the Fourier component $\alpha_{\mathbf{n},\mathrm{ai}}(\omega_{\mathrm{exc}})$ (see Fig. 2). We used DWTA to analyze all X-ray absorption resonances of SF_6 between 170 and 200 eV, and the result for the eight most

intense transitions is shown in Fig. 2. The analysis revealed the following: (1) all nonphysical peaks observed in the simulations without SP arise from excitations of electrons from non-core occupied orbitals to high-laying virtual orbitals. This observation justifies the use of SP. (2) The doublet structure originates from the spin–orbit splitting of the sulfur 2p orbitals—the lower-energy resonances correspond to promotion from $2p_{3/2}$, whereas those at higher-energies are from $2p_{1/2}$. (3) All dipole-allowed transitions can be grouped according to irreducible representations of the octahedral point group: a_{1g}, t_{2g} and e_g (Table 1).

The final calculated and experimental photoabsorption specta of SF_6 near the sulfur $L_{2,3}$-edges are depicted in Fig. 1. For clarity, the figure also provides comparison between the nonrelativistic (1-component) and the relativistic (4-component) theoretical spectra, clearly demonstrating the importance of a full spin–orbit treatment in reproducing the doublet structure of all spectral lines. The molecular resonances at 172–174 eV represent an excitation of a sulfur 2p electron to the lowest-unoccupied molecular orbital (LUMO). The LUMO is an anti-bonding $\sigma^\star$ orbital of a_{1g} symmetry, attributed primarily to the sulfur $4s_{1/2}$. The calculated spin–orbit splitting of 1.22 eV between the low-lying photoabsorption resonances, (S $2p_{1/2})^{-1}a_{1g}$ and (S $2p_{3/2})^{-1}a_{1g}$, agrees very well with the experimental observation (1.17 eV). Notably, the present theoretical model predicts correctly the declination of intensity ratio between (S $2p_{3/2})^{-1}$ and (S $2p_{1/2})^{-1}$ from 2 : 1 to 1 : 1.3. This reversed intensity ratio is a phenomenon caused by a significant exchange interaction between an electron in an inner-well excited state and the remaining sulfur core electrons.[38] The calculated ratio of 1 : 1.3 is, however, slightly below the experimental XANES ratio of 1 : 1.6.
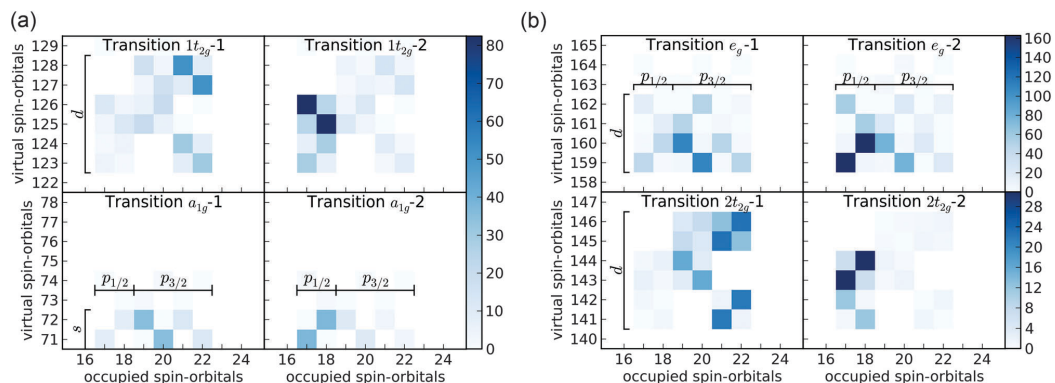
Fig. 2 The DWTA analysis of the first eight dominant transitions in the XANES spectrum of SF_6—a_{1g} (bottom left), $1t_{2g}$ (top left), $2t_{2g}$ (bottom right) and e_g (top right). The intensity of the blue color corresponds to the intensity of the particular excitation; the units in the colorbars on the right are arbitrary—only relative intensities are meaningful. The excitations are always Kramers-paired and form 2 × 2 sub-matrices. Due to an ambiguity in the phase of these spin–orbitals the internal structure of the 2 × 2 sub-matrices does not have a physical interpretation.

The second intense doublet (at 184–186 eV), just above the sulfur $L_{2,3}$ thresholds, is a molecular shape resonance, assigned to the promotion of a single sulfur 2p electron to a quasi-bound orbital of t_{2g} symmetry. The theoretical magnitude of the SO splitting (1.17 eV) matches the XANES experiment exactly. The intensity ratio of 1 : 1.19 is slightly below the experimental value 1 : 2.04. The next shape resonance is of e_g symmetry, and consists of a single wide peak in the experiment, spanning the energy range between 190–200 eV. Due to the absence of mechanisms capturing the finite lifetime of such states, we can probe by present calculation the structure of this peak in more detail. In particular, the spin–orbit splitting of the 2p orbitals is again responsible for the doublet structure of the transition (1.31 eV). Moreover, we observe an additional weaker doublet

of t_{2g} symmetry (labeled $2t_{2g}$ in the figures and the table) and a very weak doublet of a_{1g} symmetry in close proximity to the e_g transition. Ferrett et al.[39] found that the resonance also exhibits strong multielectron effects in its decay, but study of such effects is beyond the scope of this Letter. In the Rydberg region we identified three pairs of resonances with a_{1g}, e_g and t_{2g} symmetries, matching the states with excitations to lower outer-well orbitals observed experimentally. For each pair, the calculated value of the spin–orbit splitting was 1.27–1.28 eV, which is in very good agreement with the experimental observation of 1.20–1.21 eV, in particular if we consider the character of the final states—Rydberg states.

Finally, there are several factors that affect the accuracy of the simulations. Apart from the choice of the DFT functional, there are two notable sources of error responsible for the differences between the calculation and the experiment. First, intensities of Rydberg states and high-energy shape resonances were much more susceptible to changes of basis set. The poorer description of the Rydberg states is mostly due to the delocalized character of outer-well orbitals. On the other hand, the inner-well state (first a_{1g}) was perfectly described even with smaller basis sets. Second, the finite simulation time resulted in the finite resolution. The error was sufficiently small for stronger resonances, but affected the weak transitions. The intensities of the Rydberg transitions were more prone to both errors, therefore we omitted them from the comparison with the experiment.

In conclusion, we have reported the first implementation and application of relativistic four-component real-time TDDFT to the simulation of core-level near-edge X-ray absorption spectroscopy. The proposed formalism accounts variationally for relativistic corrections arising from the Dirac–Coulomb Hamiltonian, of which the spin–orbit coupling is of significant importance for reproducing the multiplet structure of the spectral lines near $L_{2,3}$ absorption edges. The computed XANES spectrum of SF_6 agrees very well with experimental results, in particular when reducing the intesity of nonphysical excitations

Table 1 Comparison of the calculated photoabsorption spectrum of SF_6 near the sulfur $L_{2,3}$-edges with the high-resolution XANES experiment[23]

Peak	Assignment[a]	Exc. energy [eV]		Intensity [arb.]	
		This work[b]	Exp.	This work	Exp.
a_{1g}−1	$a_{1g}^1(2p_{3/2})^{-1}$	172.27	172.27	1.00	1.00
a_{1g}−2	$a_{1g}^1(2p_{1/2})^{-1}$	173.49	173.44	1.35	1.62
A	$a_{1g}^1(2p_{3/2})^{-1}$	177.89	177.42	0.07	
B	$a_{1g}^1(2p_{1/2})^{-1}$	179.16	178.63	0.03	
C	$e_g^1(2p_{3/2})^{-1}$	180.00	178.80	0.03	
D	$t_{2g}^1(2p_{3/2})^{-1}$	180.56	178.76	0.16	
E	$e_g^1(2p_{1/2})^{-1}$	181.28	180.00	0.01	
F	$t_{2g}^1(2p_{1/2})^{-1}$	181.83	179.96	0.07	
$1t_{2g}$−1	$t_{2g}^1(2p_{3/2})^{-1}$	184.06	183.40	3.53	2.71
$1t_{2g}$−2	$t_{2g}^1(2p_{1/2})^{-1}$	185.23	184.57	4.21	5.53
$2t_{2g}$−1	$t_{2g}^1(2p_{3/2})^{-1}$	189.86		1.55	
$2t_{2g}$−2	$t_{2g}^1(2p_{1/2})^{-1}$	191.07		0.97	
e_g−1	$e_g^1(2p_{3/2})^{-1}$	194.98	196.2	3.80	15.7
e_g−2	$e_g^1(2p_{1/2})^{-1}$	196.29		9.80	
G	$a_{1g}^1(2p_{3/2})^{-1}$	196.87		0.05	
H	$a_{1g}^1(2p_{1/2})^{-1}$	198.12		0.09	

[a] All holes correspond to sulfur 2p spin–orbitals. [b] The simulated spectrum was shifted by 7.89 eV to account for the self-interaction error.

by the developed selective perturbation. The character of the eight most intense excitations was analyzed in terms of molecular orbitals by means of a proposed DWTA technique, and both the assignments and fine-structure splittings were found to be in good agreement with high-resolution experimental data.

Acknowledgements

References

1 H. Ågren, V. Carravetta, O. Vahtras and L. G. Pettersson, *Chem. Phys. Lett.*, 1994, **222**, 75–81.
2 P. Lee and J. Pendry, *Phys. Rev. B: Solid State*, 1975, **11**, 2795.
3 A. Ankudinov, B. Ravel, J. Rehr and S. Conradson, *Phys. Rev. B: Condens. Matter Mater. Phys.*, 1998, **58**, 7565.
4 E. E. Salpeter and H. A. Bethe, *Phys. Rev.*, 1951, **84**, 1232–1242.
5 E. L. Shirley, *Phys. Rev. Lett.*, 1998, **80**, 794.
6 A. Ankudinov, Y. Takimoto and J. Rehr, *Phys. Rev. B: Condens. Matter Mater. Phys.*, 2005, **71**, 165110.
7 T. Fransson, S. Coriani, O. Christiansen and P. Norman, *J. Chem. Phys.*, 2013, **138**, 124311.
8 O. Plekan, V. Feyer, R. Richter, M. Coreno, M. de Simone, K. Prince, A. Trofimov, E. Gromov, I. Zaytseva and J. Schirmer, *Chem. Phys.*, 2008, **347**, 360–375.
9 E. Runge and E. K. Gross, *Phys. Rev. Lett.*, 1984, **52**, 997.
10 G. Onida, L. Reining and A. Rubio, *Rev. Mod. Phys.*, 2002, **74**, 601.
11 M. Stener, G. Fronzoni and M. De Simone, *Chem. Phys. Lett.*, 2003, **373**, 115–123.
12 Y. Zhang, J. D. Biggs, D. Healion, N. Govind and S. Mukamel, *J. Chem. Phys.*, 2012, **137**, 194306.
13 U. Ekström, P. Norman, V. Carravetta and H. Ågren, *Phys. Rev. Lett.*, 2006, **97**, 143001.
14 P. Norman, D. M. Bishop, H. J. A. Jensen and J. Oddershede, *J. Chem. Phys.*, 2001, **115**, 10323–10334.
15 U. Ekström and P. Norman, *Phys. Rev. A: At., Mol., Opt. Phys.*, 2006, **74**, 042722.
16 T. Akama, Y. Imamura and H. Nakai, *Chem. Lett.*, 2010, **39**, 407–409.
17 T. Akama and H. Nakai, *J. Chem. Phys.*, 2010, **132**, 054104.
18 K. Lopata, B. E. Van Kuiken, M. Khalil and N. Govind, *J. Chem. Theory Comput.*, 2012, **8**, 3284–3292.
19 A. J. Lee, F. D. Vila and J. J. Rehr, *Phys. Rev. B: Condens. Matter Mater. Phys.*, 2012, **86**, 115107.
20 B. Gao, K. Ruud and Y. Luo, *J. Chem. Phys.*, 2012, **137**, 194307.
21 S. Selstø, E. Lindroth and J. Bengtsson, *Phys. Rev. A: At., Mol., Opt. Phys.*, 2009, **79**, 043418.
22 L. Belpassi, L. Storchi, H. M. Quiney and F. Tarantelli, *Phys. Chem. Chem. Phys.*, 2011, **13**, 12368–12394.
23 E. Hudson, D. A. Shirley, M. Domke, G. Remmers, A. Puschmann, T. Mandel, C. Xue and G. Kaindl, *Phys. Rev. A: At., Mol., Opt. Phys.*, 1993, **47**, 361–372.
24 R. Kosloff, *J. Phys. Chem.*, 1988, **92**, 2087–2100.
25 A. Castro, M. a. L. Marques and A. Rubio, *J. Chem. Phys.*, 2004, **121**, 3425–3433.
26 W. Magnus, *Commun. Pure Appl. Math.*, 1954, **7**, 649–673.
27 M. Repisky, L. Konecny, M. Kadek, S. Komorovsky, O. L. Malkin, V. G. Malkin and K. Ruud, *J. Chem. Theory Comput.*, 2015, **11**, 980–991.
28 ReSpect, version 3.4.2, 2015 – Relativistic Spectroscopy DFT Program of Authors: M. Repisky, S. Komorovsky, V. G. Malkin, O. L. Malkina, M. Kaupp, K. Ruud, with contributions from R. Bast, U. Ekstrom, M. Kadek, S. Knecht, L. Konecny, I. Malkin Ondik and E. Malkin, see www.respectprogram.org.
29 A. D. Becke, *J. Chem. Phys.*, 1993, **98**, 5648–5652.
30 C. Lee, W. Yang and R. G. Parr, *Phys. Rev. B: Condens. Matter Mater. Phys.*, 1988, **37**, 785.
31 G. Herzberg, *Molecular spectra and molecular structure. Vol. 3: Electronic spectra and electronic structure of polyatomic molecules*, Van Nostrand Reinhold, New York, 1966.
32 T. H. Dunning, *J. Chem. Phys.*, 1989, **90**, 1007.
33 R. E. Stanton and S. Havriliak, *J. Chem. Phys.*, 1984, **81**, 1910–1918.
34 T. H. Dunning, K. A. Peterson and A. K. Wilson, *J. Chem. Phys.*, 2001, **114**, 9244–9253.
35 R. A. Kendall, T. H. Dunning and R. J. Harrison, *J. Chem. Phys.*, 1992, **96**, 6796.
36 J. D. Hunter, *Comput. Sci. Eng.*, 2007, **9**, 90–95.
37 J. P. Perdew, R. G. Parr, M. Levy and J. L. Balduz Jr, *Phys. Rev. Lett.*, 1982, **49**, 1691.
38 J. L. Dehmer, *J. Chem. Phys.*, 1972, **56**, 4496–4504.
39 T. Ferrett, D. Lindle, P. Heimann, M. Piancastelli, P. Kobrin, H. Kerkhoff, U. Becker, W. Brewer and D. Shirley, *J. Chem. Phys.*, 1988, **89**, 4726–4736.

22570 | *Phys. Chem. Chem. Phys.*, 2015, **17**, 22566–22570

This journal is © the Owner Societies 2015